Crystal Structure of S-Ribosylhomocysteinase (LuxS) in Complex with a Catalytic 2-Ketone Intermediate[†,‡]

Rakhi Rajan, Jinge Zhu, Xubo Hu, Dehua Pei, and Charles E. Bell*

Department of Molecular and Cellular Biochemistry, Department of Chemistry, Biophysics Program, and Ohio State Biochemistry Program, The Ohio State University, Columbus, Ohio 43210

Received October 22, 2004; Revised Manuscript Received December 22, 2004

ABSTRACT: *S*-Ribosylhomocysteinase (LuxS) is an Fe^{2+}-dependent metalloenzyme that catalyzes the cleavage of the thioether bond in *S*-ribosylhomocysteine (SRH) to produce homocysteine (Hcys) and 4,5-dihydroxy-2,3-pentanedione (DPD), the precursor of type II bacterial quorum-sensing molecule. The proposed mechanism involves an initial metal-catalyzed aldose-ketose isomerization reaction, which results in the migration of the ribose carbonyl group from its C1 to C2 position and the formation of a 2-ketone intermediate. A repetition of the isomerization reaction shifts the carbonyl group to the C3 position. Subsequent β-elimination reaction at the C4 and C5 positions completes the catalytic cycle. In this work, a catalytically inactive mutant (C84A) of Co^{2+}-substituted *Bacillus subtilis* LuxS was cocrystallized with the 2-ketone intermediate and the structure was determined to 1.8 Å resolution. The structure reveals that the C2 carbonyl oxygen is directly coordinated with the metal ion, providing strong support for the proposed Lewis acid function of the metal ion during catalysis. Cys-84 and Glu-57 are optimally positioned to act as general acids/bases during the isomerization and elimination reactions. In addition, Ser-6, His-11, and Arg-39 are involved in substrate/ intermediate binding through hydrogen bonding interactions. The above conclusions are further confirmed by site-directed mutagenesis and visible absorption spectroscopic studies.

S-Ribosylhomocysteinase (LuxS) is the key enzyme on the biosynthetic pathway of type II autoinducer (AI-2),[1] which mediates the interspecies quorum sensing among both Gram-positive and Gram-negative bacteria (*1*, *2*). The biosynthesis starts from *S*-adenosylhomocysteine (SAH), which is formed as a byproduct of many *S*-adenosylmethionine-dependent methyltransferase reactions (Figure 1). SAH is hydrolyzed by a nucleosidase Pfs to adenine and *S*-ribosylhomocysteine (SRH). Next, LuxS cleaves the thioether bond in SRH to produce l-homocysteine (Hcys) and 4,5-dihydroxy-2,3-pentanedione (DPD) (*3*−*5*). DPD spontaneously cyclizes to form a furanone as the active form of AI-2 molecule in *Salmonella typhimurium* (*6*). In *Vibrio harveyi* the furanone is further complexed with borate to produce a furanosylborate diester as active AI-2 (*7*).

The reaction catalyzed by LuxS is mechanistically fascinating. Although the overall reaction is analogous to the reaction catalyzed by SAH hydrolase, which hydrolytically cleaves SAH into Hcys and adenosine, LuxS does not contain the essential NAD^+ cofactor found in SAH hydrolase (*8*). Instead, the high-resolution X-ray crystal structures of LuxS from *Bacillus subtilis*, *Helicobacter pylori*, Haemophilus influenzae, and *Deinococcus radiodurans* revealed that LuxS contains a tetrahedrally bound divalent metal in the active site (*9*−*11*). Biochemical studies have shown that the divalent metal ion is Fe^{2+} in LuxS from *B. subtilis* and likely other bacterial species, although substitution of Co^{2+} retains full catalytic activity (*12*). LuxS exists as a homodimer and two identical active sites are formed at the dimer interface. Each active site contains an Fe^{2+} ion, coordinated by three conserved residues [His-54, His-58, and Cys-126 in *B.*

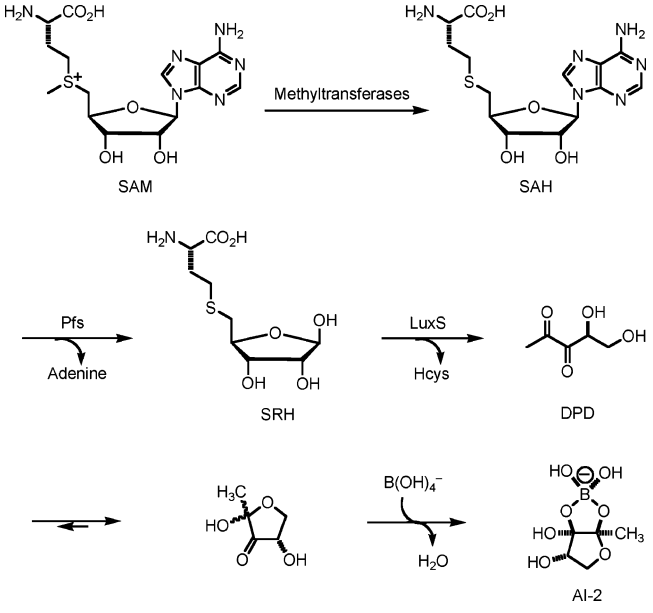

FIGURE 1: Biosynthetic pathway of AI-2.

[†] This work was supported by grants from the National Institutes of Health (GM62820 and AI40575).

[‡] The coordinates for the structure of LuxS in complex with the 2-ketone intermediate have been deposited in the Protein Data Bank under accession number HPUB.

* To whom correspondence should be addressed. Phone: (614) 688-3115; Fax: (614) 292-4118; E-mail: bell.489@osu.edu.

[1] Abbreviations: AI, autoinducer; SAH, *S*-adenosylhomocysteine; SAM, S-adenosylmethionine; SRH, *S*-ribosylhomocysteine; Hcys, homocysteine; DPD, 4,5-dihydroxy-2,3-pentanedione; DTNB, 5,5′-dithio-bis-(2-nitrobenzoic acid); BsLuxS, *B. subtilis* LuxS.; VhLuxS, *V. harveyi* LuxS.

10.1021/bi0477384 CCC: $30.25
Published on Web 02/11/2005

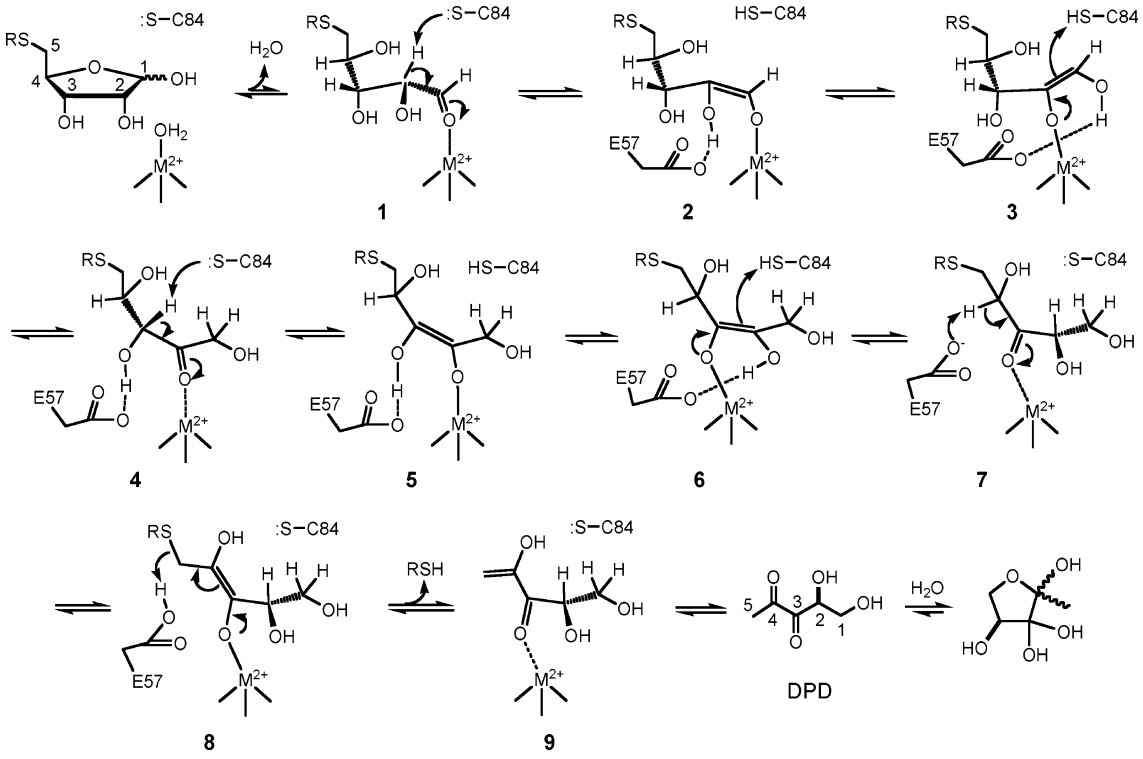

FIGURE 2: Proposed catalytic mechanism of LuxS. RSH, L-homocysteine.

subtilis LuxS (BsLuxS)] and a water molecule. A catalytic mechanism has recently been proposed for the LuxS-catalyzed reaction, as shown in Figure 2 (*12*−*14*). In an aqueous solution, the ribose ring of SRH is in equilibrium with the open-chain, free aldehyde form. LuxS may either preferentially bind the open-chain form and shift the equilibrium or bind the ribose form and catalyze its ring opening. In the productive E•S complex **1**, the aldehyde carbonyl binds to the metal ion, displacing a bound water/hydroxide in the free enzyme. Coordination to the metal increases the acidity of the C2 proton, which is abstracted by a general base (likely Cys-84 in BsLuxS). The cis-enediolate **2** formed undergoes ligand exchange, shifting the metal from C1 to the C2 OH group, presumably assisted by a second base/acid (likely Glu-57) and via a five-membered-ring transition state, to give enediolate **3**. Reprotonation at C1 position by Cys-84 and tautomerism back to the keto form generate a 2-keto intermediate **4**. Repetition of the above sequence shifts the carbonyl group to C3 position to give a 3-keto intermediate **7**. Subsequent β-elimination, probably catalyzed by Glu-57 (or possibly a third acid/base), results in the release of Hcys and the formation of DPD in its enol form **9**. Enol **9** spontaneously tautomerizes to the keto form, either on its way off or after leaving the active site.

The above mechanism is supported by several lines of evidence. When the LuxS reaction was carried out in D_2O, deuterium was incorporated into C1, C2, and C5 positions of DPD, establishing the involvement of proton transfers in the mechanism (*12*). Both the regiochemistry and stereochemistry of the proton transfer steps in Figure 2 have recently been confirmed experimentally by using specifically deuterated SRH substrates (*14*). The ketone intermediates **4** and **7** have been observed in real time by ^{13}C NMR spectroscopy (*13*). Furthermore, the 2-keto intermediate has been chemically synthesized and demonstrated to be a chemically and kinetically competent intermediate on the catalytic pathway (*13*). Despite significant progresses made during the past few years, some mechanistic issues still remain unresolved. One issue is the role of the metal ion during catalysis. The dramatic catalysis-dependent changes in the absorption spectra of the Co^{2+}-substituted LuxS suggest that the metal ion is directly coordinated with the substrate/intermediates (*12*). However, in the cocrystal structure of LuxS bound to SRH, the ribose hydroxyl groups were 3.0 and 3.2 Å away from the metal ion, ruling out direct coordination of the metal ion by the hydroxyl groups (*11*). Another unresolved issue is the function of Ser-6, His-11, and Arg-39, which are in close proximity to the substrate and are highly conserved residues. Interpretation of the reported LuxS/SRH structure was potentially complicated by several factors. First, the solved structure contained a Zn^{2+} ion as the metal cofactor and the Zn^{2+}-LuxS is an order of magnitude less active than the native enzyme. Second, Cys-84 in the structure was oxidized into cysteic acid, whose larger size undoubtedly affects substrate binding and catalysis. Indeed, oxidation of Cys-84 to cysteic acid inactivates LuxS (*12*). Third, the reported structure had relatively high *B*-factors for the metal ion and SRH, apparently arising from their partial occupancy in the active site, as well as an alternative conformation for the O1 ribose hydroxyl group (β-conformer) of the substrate. Finally, the ribose form of SRH is not the "active" form of the substrate and, therefore, the structure does not reflect that of the productive E•S complex. In this work, we crystallized a catalytically inactive Cys84Ala mutant form of BsLuxS in complex with the chemically synthesized ketone intermediate **4**. The Cys84Ala substitution is necessary to prevent turnover of the intermediate by LuxS. The structure shows that the 2-keto group is directly coordinated with the metal ion, thus providing strong evidence for the proposed Lewis acid function of the metal

ion. In addition, site-directed mutagenesis studies show that Ser-6, His-11, and Arg-39 are critical residues for substrate binding and catalysis. The cocrystal structure provides a mechanistic explanation for their critical roles in catalysis.

MATERIALS AND METHODS

Materials. Oligonucleotides were purchased from Integrated DNA Technologies (Coralville, IA). Talon resin was from Clontech Laboratories (Palo Alto, CA). The 2-ketone intermediate **4** was synthesized as previously described (*13*). The chemicals used in crystal growth and handling were Fisher Scientific certified A.C.S.-grade. All other chemicals were purchased from Sigma-Aldrich (St. Louis, MO).

Site-Directed Mutagenesis of LuxS. Site-directed mutagenesis was carried out on the plasmids pET22b-luxS (non-His-tag) for BsLuxS (*12*) and pET22b-luxS−HT for *V. harveyi* LuxS (VhLuxS) (*13*) using the QuikChange mutagenesis kit (Stratagene, CA). The primers used were as follows: BsLuxS−C84A, 5′-GATATTTCTCCAATGGGCGCCCAAACAG-GCTATTATC-3′; VhLuxS−S6A, 5′-ATGCCTTTATTA-GACGCCTTTACCGTA-3′; VhLuxS−H11Q, 5′-AGCTTTACCGTAGACCAAACGCGTAT-3′; VhLuxS−R39M, 5′-ACGGTATTCGACCTAATGTTCACTGC-3′; and VhLuxS−R39K, 5′-ACGGTATTCGACCTAAAATTCACT-GC-3′. The identity of all DNA constructs was confirmed by DNA sequencing.

Purification of C84A BsLuxS (Non-His-Tag). E. coli BL21(DE3) cells (4 L) carrying the plasmid pET22b-luxS-C84A were grown in minimal media supplemented with 75 mg/L ampicillin, 0.25% d-glucose, 2 μg/mL thiamin, 1 μg/ mL D-biotin, 0.1% $(NH_4)_2SO_4$, and a metal salt mixture (0.5 mM $MgSO_4$, 0.5 μM H_3BO_3, 0.1 μM $MnCl_2$, 0.5 μM $CaCl_2$, 10 nM $CuSO_4$, 1 nM ammonium molybdate) at 37 °C to an OD_{600} of 0.6. The cells were induced by the addition of 100 μM isopropyl β- D-thiogalactoside, and continued to grow at 30 °C for an additional 15 h. For the preparation of Co^{2+}-substituted enzymes, 100 μM $CoCl_2$ was added to the growth media at the time of induction. Cells were harvested by centrifugation and resuspended in 70 mL of lysis buffer containing 25 mM Tris (pH 7.6), 20 mM NaCl, 1% Triton X-100, 0.5% protamine sulfate, 40 μg/mL *p*-methylbenzenesulfonyl fluoride and 70 μg/mL chicken egg white lysozyme. The cells were lysed by stirring for 20 min at 4 °C, followed by brief sonication and centrifugation. The supernatant was loaded on a Q-Sepharose Fast-Flow column (2.5 × 13 cm; Amersham Pharmacia Biotech AB) preequilibrated with 25 mM Tris (pH 7.6) and 20 mM NaCl. The column was washed with 300 mL of the equilibrating buffer and eluted with a NaCl gradient (20−500 mM) in the above buffer. Purple fractions containing significant amount of LuxS protein (as analyzed by SDS−PAGE) were pooled (80 mL), concentrated in an Amicon apparatus (Millipore) to 33 mL and adjusted to 1 M $(NH_4)_2SO_4$. The protein solution was then loaded on a Phenyl-Sepharose Fast-Flow column (2.5 × 16 cm; Amersham Pharmacia Biotech AB), washed with 80 mL of equilibrating buffer containing 25 mM Tris (pH 7.8), 20 mM NaCl and 1 M $(NH_4)_2SO_4$, and eluted with a reverse gradient of 1−0 M $(NH_4)_2SO_4$. Fractions were analyzed by 15% SDS−PAGE, concentrated to 20 mL, quickly frozen in 2-propanol dry ice bath and stored at −80 °C. Protein concentration was determined by the Bradford method using bovine serum albumin as standard and by measuring the thiol content using 5,5′-dithio-bis-(2-nitrobenzoic acid) (DTNB) (*15*). Metal analysis was performed by inductively coupled plasma emission spectrometry (ICP-ES) at the Chemical Analysis Laboratory of the University of Georgia. C84A LuxS contained 0.89 Co and 0.02 Zn per polypeptide. The results showed that the Bradford method overestimates the LuxS concentration by a factor of 2.5, a fact that was corroborated by the metal analysis results (ref 12 and this work).

Purification of VhLuxS Mutants. E. coli BL21(DE3) cells (4 L) carrying the appropriate plasmid DNAs were grown in the above media at 37 °C to an OD_{600} of 0.9. Cells were induced in the same manner for 5 h at 30 °C in the presence of 100 μM $CoCl_2$. After centrifugation, cells were lysed in 70 mL of lysis buffer containing 20 mM Tris (pH 8.0), 0.5 M NaCl, 5 mM imidazole, 1% Triton X-100, 0.5% protamine sulfate, and 70 μg/mL chicken egg white lysozyme with stirring and brief sonication. After spinning down the crude lysate, the supernatant was loaded on a Talon metal affinity column (Clontech, 2.5 × 2.5 cm) equilibrated in 20 mM Tris (pH 8.0), 0.5 M NaCl, and 5 mM imidazole. The column was eluted with the above buffer containing 60 mM imidazole. Fractions were colleted, analyzed and stored in the same manner as described above. Protein concentration was determined by Bradford method and corrected by a factor of 0.5, which is based on the metal analysis results of *V. harveyi* Co^{2+}-LuxS.

LuxS Activity Assay. All LuxS activity assays were performed in a buffer containing 50 mM HEPES (pH 7.0), 150 mM NaCl, 150 μM DTNB (*15*) and various concentrations of SRH (0−200 μM) or 2-ketone **4** (0−130 μM) at room temperature. The reactions were initiated by the addition of Co^{2+}−LuxS (final concentration 0.5−1.7 μM) and monitored continuously at 412 nm in a Perkin-Elmer λ25 UV−vis spectrophotometer. The initial rates recorded from the early regions of the progress curves were fitted into the Michaelis−Menten equation using KaleidaGraph 3.5 to obtain the k_{cat} and K_M values.

UV−Vis Spectroscopy. C84A BsLuxS (non-His-tag) was diluted in a buffer containing 50 mM HEPES (pH 7.0) to give a final concentration of 220 μM, and incubated with 370 μM of 2-ketone **4** at room temperature. Absorption spectra were recorded on a Perkin-Elmer λ25 UV−vis spectrophotometer at various times (0−90 min).

Crystallization and Structure Determination. The C84A variant of BsLuxS was cocrystallized with 2-ketone intermediate **4** by hanging drop vapor diffusion, where the well solution consisted of 2.2 M ammonium sulfate, 0.1 M HEPES pH 7.0, and the hanging drop was prepared by mixing 2 μL of well solution with 2 μL of 35 mg/ mL (1.9 mM) LuxS, 3 mM intermediate **4**, 25 mM Tris pH 8.0, 100 mM sodium chloride. Prior to data collection crystals were transferred to a solution of 15% glycerol, 2.5 M ammonium sulfate, 0.1 M HEPES pH 7.0, 3 mM intermediate **4**, mounted in nylon loops (Hampton Research), and frozen by plunging in liquid nitrogen. X-ray diffraction data were collected at −180 °C using a Rigaku RUH3RHB rotating anode generator and an R-AXIS IV++ image plate detector. The data were processed with CrystalClear software (Molecular Structure Corporation). Crystallographic refinement using

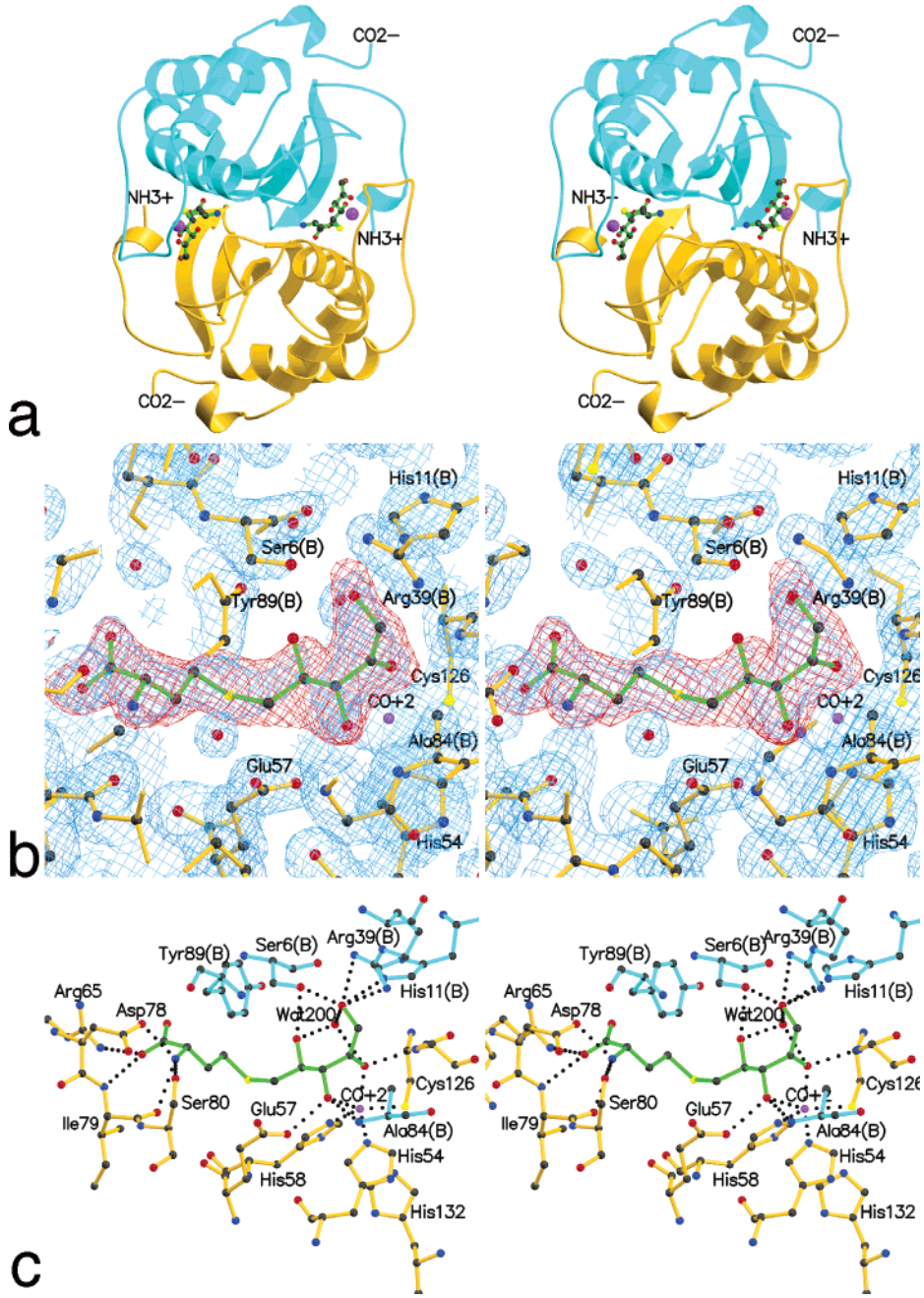

FIGURE 3: Crystal structure of LuxS in complex with the 2-ketone intermediate 4: (A) Stereo ribbon drawing of the LuxS dimer bound to the 2-ketone intermediate. The two intermediate compounds are bound at the interface and shown in ball-and-stick with green bonds. The Co^{2+} ions of each active site are shown as purple spheres. The N- and C-terminal residues of the model (Val-4 and Gly-157) are indicated. (B) Stereoview of electron density in the active site region. The view is approximately the same as for the active site on the right of the dimer in panel A. The blue cage is the 1.8 Å $2F_{obs} - F_{calc}$ electron density map contoured at 1 σ. The red cage is a 1.8 Å $F_{obs} - F_{calc}$ simulated annealing omit map contoured at 3.5 σ, for which the atoms of the 2-ketone intermediate were omitted for the refinement and map calculation. (C) Stereoview of the atomic interactions between LuxS and the 2-ketone intermediate. Amino acid residues of subunit A of the dimer, which has the bound Co^{2+} ion for this active site, are shown with gold bonds. Amino acid residues of the other subunit (B) are shown with cyan bonds. Atom types are colored as follows: oxygen, red; carbon, black; nitrogen, blue, sulfur, yellow; cobalt, purple. All potential hydrogen bonds within 3.5 Å are shown as dotted lines. Notice that the oxygen atom of the 2-ketone position of the intermediate is coordinated to the cobalt ion. Also notice that the Ala-84 Cβ atom of the Cys-84Ala LuxS protein is positioned near the C2 and C3 atoms of the 2-ketone intermediate.

CNS (*16*) began with the structure of the BsLuxS SRH complex (PDB code 1JVI) (*11*) with all water molecules and SRH omitted and Cys-84 truncated to alanine. The conjugate gradient minimization and individual temperature factor protocols were used with a maximum likelihood target and overall anisotropic temperature factor and bulk solvent corrections to the data. The 2-ketone intermediate was added to the model at the later stages of refinement after all of the protein atoms and several water molecules were positioned. Model building used the program O (*17*), and the geometrical parameters for refinement of the 2-ketone intermediate were generated using the Dundee PRODRG2 server (*18*). The distances between the Co^{2+} and its protein and substrate ligands were not restrained. Figures were generated using O, MOLSCRIPT (*19*), RASTER3D (*20*), and LIGPLOT (*21*).

Table 1: Data Collection and Refinement Statistics

Data Collection Statistics	
space group	$P6_522$
a = b (Å)	62.5
c (Å)	149.7
resolution (Å)	16.1-1.8
no. of reflns	205,678
no. of unique reflns	17,419
completeness (%)	99.6 (97.3)[a]
redundancy	11.8 (8.9)
R_{merge} (%)[b]	9.9 (53.4)
I/σ[c]	12.7 (4.1)
Refinement Statistics	
resolution (Å)	16.1-1.8
no. of reflns (working/free)	15,098/1,638
completeness (%)	99.7
mean *B*-factor (Å^2)	29.0
estimated coordinate error[d]	0.35
R factor	22.5 (42.1)
R_{free} (%)[e]	25.6 (42.4)
no. waters	103
RMS Deviation from Ideal Geometry	
bonds (Å)	0.006
angles (°)	1.2 3

[a] Numbers in parentheses refer to the highest resolution shell only. [b] $R_{merge} = \sum|I_h - \langle I\rangle_h|/\sum_h$, where $\langle I\rangle_h$ is average intensity over symmetry equivalents. [c] I/σ is the mean of the intensity/sigma of the unique, averaged reflections. [d] The estimated coordinate error is the value from the cross-validated $\sum$ plot. [e] *R* factor $= \sum|F_{obs} - F_{calc}|/\sum_{obs}$. R_{free} is calculated from 10% of the reflections that are omitted from the refinement.

RESULTS AND DISCUSSION

Structure of LuxS Complexed with Catalytic 2-Ketone Intermediate. The catalytically inactive C84A variant of *B. subtilis* LuxS (*12*, *13*) was cocrystallized with 2-ketone intermediate **4** from solutions of ammonium sulfate at pH 7.0. The crystals are the same form as previously reported for BsLuxS (*10*, *11*), space group $P6_522$ with one LuxS subunit and one 2-ketone intermediate per asymmetric unit. The two subunits of the LuxS molecular dimer are related by a crystallographic 2-fold axis of symmetry with two identical active sites formed at the dimer interface (Figure 3a). The structure was refined at 1.8 Å resolution to an R-factor and free R-factor of 22.5% and 25.6%, respectively (Table 1). The model includes all residues of LuxS except for residues 1−3 at the N-terminus, for which there was no observed electron density. The estimated atomic coordinate error of the structure is 0.20−0.35 Å.

The 1.8 Å resolution diffraction limit of the crystals of the complex reported here, which is the best that could be obtained after several trials, is somewhat lower than the 1.2 Å (PDB code 1J98) or 1.6 Å (PDB code 1IEO) diffraction limit for crystals of uncomplexed BsLuxS (*10*−*11*), but higher than the 2.2 Å diffraction limit for crystals of BsLuxS in complex with SRH (PDB code 1JVI) (*11*). For all four structure determinations, the diffraction data were collected on similar rotating anode sources, thus the diffraction limit likely reflects an increase in flexibility and/ or conformational heterogeneity of the protein upon substrate binding, which is more prevalent in the complex with SRH than in the complex with the 2-ketone intermediate. Accordingly, the mean temperature factor value of 29 Å^2 for the structure of the complex with the 2-ketone intermediate is between that of the structure of uncomplexed BsLuxs (19 Å^2) and BsLuxS bound to SRH (37 Å^2) (*11*).

The presence of the bound 2-ketone intermediate causes only very slight structural changes in the LuxS dimer, which can be superimposed to the 1.2 Å structure of the uncomplexed LuxS dimer (*11*; PDB code 1J98) to an rmsd of 0.23 Å for all Cα atoms. Despite the fact that the active sites are located at the interface between the two subunits of the dimer, binding of the 2-ketone intermediate does not cause any significant changes in the protein−protein interactions at the interface. The largest differences between the two structures are on the order of ∼1 Å and occur at Arg-65 and Pro-96. Arg-65, which is at a kink in helix α1, interacts with the carboxylate of the homocysteine moiety of the 2-ketone intermediate and is pulled toward the active site by about 1.2 Å in the structure of the complex reported here as well as in the complex with SRH (*11*). Pro-96 of LuxS is modeled as Thr in the 1.2 Å structure of uncomplexed BsLuxS as well as in the complex with SRH (*11*), but is clearly present as Pro in the current structure, resulting in ∼1.2 Å shifts of the backbone atoms.

The electron density for the 2-ketone intermediate is complete (Figure 3b), allowing for placement of all of its constituent atoms. Figure 3c shows a close up view of the interactions between LuxS and the 2-ketone intermediate, and a schematic view indicating the distances between interacting atoms in the refined model is shown in Figure 4. The refined temperature factors for the 2-ketone intermediate (40−50 Å^2) are only slightly higher than for the protein atoms (20−40 Å^2), indicating full or nearly full occupancy of the compound. The Co^{2+} ion refines to a temperature factor of 32 Å^2. Like SRH, the 2-ketone intermediate is deeply buried at the dimer interface of LuxS, forming close, specific interactions with both subunits of the dimer. The homocysteine group of the 2-ketone intermediate is bound in essentially the same way to LuxS as observed for bound SRH (*11*), with the amino and carboxylate groups neutralized by interactions with the side chains of Asp-78(A) and Arg-65(A), respectively. The (A) following the residue number designates the subunit of the active site with the bound Co^{2+} ion, whereas residues of the other subunit are designated (B).

By contrast, the ribulose moiety of the 2-ketone intermediate is bound in a very different way to the enzyme than is seen for the substrate SRH (*11*). Instead of the closed ribose ring of SRH (Figure 5a), the 2-ketone intermediate is clearly in an open, extended conformation, with O4 separated from C1 by 3.5 Å. At the end of the 2-ketone intermediate, the O1 atom is anchored to the active site of LuxS through close interactions with Arg-39(B), His-11(B), and Ser-6(B), three residues that are highly conserved among all known LuxS sequences. The interactions involving His-11(B) and Arg-39(B) are not seen in the complex with SRH, in which the O1 atom is positioned differently by about 3.4 Å. The O1 atom of the 2-ketone intermediate is also within 3.6 Å of the hydroxyl group of Tyr-89(B), another highly conserved residue of LuxS.

The electron density for Ala-84(B), the site of the inactivating C84A substitution, is consistent with Ala (Figure 3b), providing further confirmation of the presence of the substitution. In structures of wild-type LuxS, the cysteine residue at this position is oxidized to sulfinic/sulfonic acid, which inactivates the enzyme (*9*−*11*). The Cβ atom of Ala-

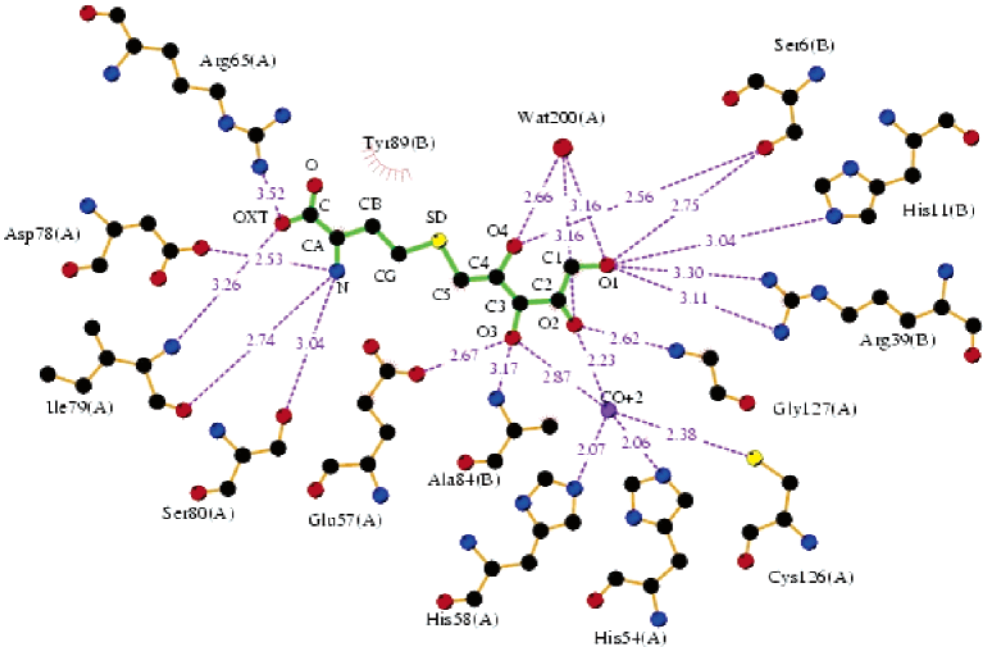

FIGURE 4: Schematic view of the interactions between LuxS and the 2-ketone intermediate. Potential hydrogen bonding interactions within 3.5 Å are shown as dashed lines with each distance indicated. Residues within van der Waals contact are also indicated. Notice that the O2 atom of 2-ketone group of the intermediate is within 2.2 Å of the Co^{2+} ion. The mean coordinate error of the crystallographic model is estimated to be 0.2−0.35 Å. The figure was prepared using LigPlot (*21*).

84 is within van der Waals contact (3.4 Å) of the C1 and C2 atoms of the 2-ketone intermediate. Thus, based on the structure of the 2-ketone intermediate bound to the C84A protein, the −SH group of Cys-84 in the wild type enzyme would be positioned to potentially interact with the C1, C2, C3, or O3 atoms of the intermediate, consistent with its proposed general acid/base roles during catalysis (Figure 2).

Moving along the 2-ketone intermediate, the O2 atom of the ketone group is oriented to form a close interaction (2.2 Å) with the Co^{2+} ion, which is also liganded by His-54(A), His-58(A), and Cys-126(A), with approximate tetrahedral coordination geometry maintained. The positions of the Co^{2+} ion and its protein ligands are not significantly altered by the binding of the 2-ketone intermediate, as compared to the 1.2 Å structure of uncomplexed BsLuxS with Zn^{2+} (*11*). The O2 atom of the 2-ketone group occupies approximately the same position as the water molecule that is the fourth ligand to the Zn^{2+} in the structure of uncomplexed BsLuxS (Figure 5b). The O2 atom of the 2-ketone group of the intermediate also interacts with the backbone amide of Gly-127(B) and a well-ordered water molecule. The O3 atom of the 2-ketone intermediate is also near the cobalt ion (2.9 Å) although it is not oriented directly toward it. The O3 atom also interacts with the carboxylate of Glu-57(A), and the backbone amide of Ala-84(B). On the basis of the retained tetrahedral geometry of the metal center and minimal spectral changes of the Co^{2+} ion upon binding of the intermediate, we conclude that the O3 atom of intermediate **4** is not directly coordinated with the metal ion. The O4 atom of the 2-ketone intermediate points away from the Co^{2+} ion, interacting with the side chain of Ser-6(B) and a water molecule.

Interestingly, a well-ordered water molecule (Wat-200) occupies the same position as the O1 atom of the SRH substrate bound to LuxS. This water forms close interactions with the side chain of Ser-6(B), the backbone carbonyl oxygen of Gln-125(A), and the O1 and O4 atoms of the 2-ketone intermediate. This water molecule is shielded from bulk solvent by the side chain of Phe-7(B), which is invariant. Conceivably, this water molecule could have a role in shuttling protons among the various groups of the enzyme and substrate during the LuxS reaction.

Site-Directed Mutagenesis. The potential roles of Ser-6, His-11, and Arg-39 in substrate/intermediate binding and catalysis were further investigated by site-directed mutagenesis. VhLuxS was chosen for the study because its higher k_{cat} value of 0.40 s^{-1} compared to 0.03 s^{-1} of BsLuxS facilitates the activity measurements. The S6A mutant showed ~14-fold lower activity toward SRH, primarily due to a decrease in k_{cat} value (0.031 s^{-1}); the K_M value (45 μM) was essentially unchanged (Table 2). The other mutants (H11Q, R39M, and R39K) had ~1,000-fold reduction in activity (k_{cat}/K_M = 8−11 M^{-1} s^{-1}). However, their k_{cat} and K_M values could not be accurately determined due to the low activities. The activity of these mutants toward the 2-ketone intermediate **4** was also assessed and compared to that of the wild-type enzyme (Table 2). Mutation of Ser-6 resulted in ~9-fold reduction in activity (k_{cat} = 0.10 s^{-1}), whereas the H11Q and R39M/K mutations reduced the activity by ~50-fold (k_{cat} ~ 0.009 s^{-1}). Again, the reduction in activity is primarily due to a decrease in k_{cat} values. Thus, Ser-6, His-11, and Arg-39 are all involved in substrate/intermediate binding and/or catalysis. Furthermore, the different magnitude in activity reduction toward SRH versus the 2-ketone intermediate indicates that these residues play important roles both in the formation and the decay of the 2-ketone intermediate.

UV−Vis Spectroscopy. The interaction of the 2-ketone intermediate with the LuxS active site was further investigated by absorption spectroscopy of Co^{2+}-substituted C84A LuxS. The spectrum of Co^{2+} ion is highly sensitive to its ligand environment, both the number and identity of the ligands as well as the ligand geometry (*22*). In the absence

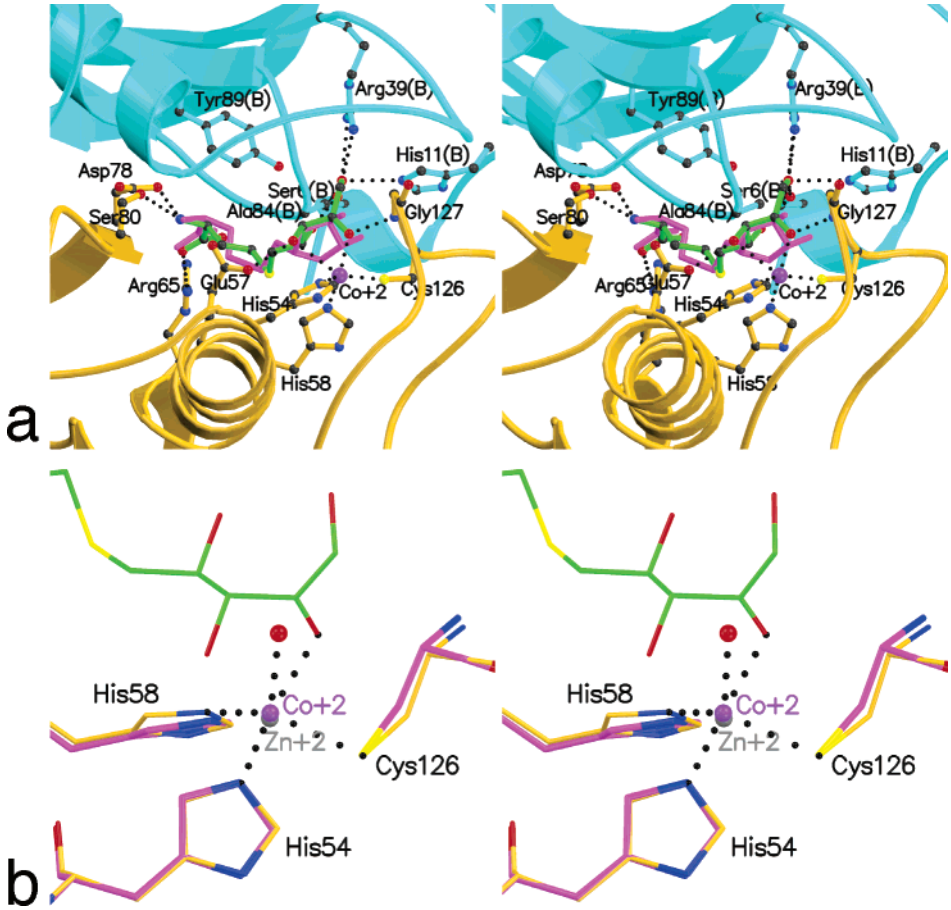

FIGURE 5: Comparison of the structure of LuxS bound to 2-ketone intermediate **4** with the structures of LuxS bound to SRH and uncomplexed LuxS: (A) The structure of LuxS bound to 2-ketone intermediate **4** (ball-and-stick with green bonds) is superimposed on SRH (magenta bonds) from the structure of the BsLuxS bound to SRH (PDB code 1JVI) (*11*). The superposition is based on all Cα atoms of the LuxS dimer for each structure. The view is approximately the same as that for Figure 3b,c. Notice that the difference in the conformation of the substrates is greatest for the O1 atom. (B) Superposition of the metal centers in the structures of LuxS with Co^{2+} bound to 2-ketone intermediate **4** (protein ligands in gold bonds) and uncomplexed LuxS with Zn^{2+} (protein ligands in magenta bonds). The water molecule (red sphere) is from the structure of uncomplexed LuxS (PDB code 1J98) (*11*).

Table 2: Catalytic Activity of LuxS Mutants

	SRH			2-ketone		
	k_{cat} (s^{-1})	K_M (μM)	k_{cat}/K_M ($M^{-1}\,s^{-1}$)	k_{cat} (s^{-1})	K_M (μM)	k_{cat}/K_M ($M^{-1}\,s^{-1}$)
WT (Bs)	0.030 ± 0.005	1.4 ± 0.1	2.1×10^4	0.031 ± 0.004	1.5 ± 0.3	2.1×10^4
WT (Vh)	0.40 ± 0.01	39 ± 1	1.0×10^4	0.40 ± 0.02	38 ± 1	1.0×10^4
E57D (Vh)[a]	NA[b]	NA[b]	118	0.008 ± 0.001	29 ± 2	2.8×10^2
C83D (Vh)[a]	NA[b]	NA[b]	4	0.005 ± 0.001	50 ± 4	1.1×10^2
C83S (Vh)[a]	NA[b]	NA[b]	14	0.024 ± 0.001	58 ± 3	4.1×10^2
S6A (Vh)	0.031 ± 0.001	45 ± 2	6.9×10^2	0.102 ± 0.002	96 ± 7	1.1×10^3
R39K (Vh)	NA[b]	NA[b]	11	0.009 ± 0.001	44 ± 1	2.0×10^2
R39M (Vh)	NA[b]	NA[b]	8	0.008 ± 0.001	22 ± 2	3.5×10^2
H11Q (Vh)	NA[b]	NA[b]	10	0.008 ± 0.001	39 ± 2	2.0×10^2

[a] Data from ref 13. [b] NA, not determined.

of the 2-ketone at pH 7.0, C84A LuxS exhibited three d−d transition bands at 660, 630, and 556 nm. The extinction coefficient for the 660 nm band, which is the strongest absorption band, is ~430 M^{-1} cm^{-1}, consistent with a tetrahedral ligand environment (Figure 6). Note that the spectrum is somewhat different than that of wild-type or E57A mutant LuxS (*12*), likely due to the removal of the negative charge associated with the thiolate ion of Cys-84. Upon the addition of 1.7 equivalents of the 2-ketone intermediate, the spectra underwent immediate changes. First, three d−d transition bands showed a decrease in intensity, with a maximum extinction coefficient of ~340 M^{-1} cm^{-1} at 660 nm. Second, the band at 556 nm was blue shifted to 548 nm. These results are consistent with the observations from the cocrystal structure that the metal ion remains tetrahedrally coordinated with His-54, His-58, Cys-126, and the carbonyl oxygen of the 2-ketone intermediate, which replaces the water in the free enzyme as the fourth ligand.

Mechanistic Implications. Central to the proposed mechanism of LuxS reaction is the Lewis acid function of the metal ion (Figure 2). Previous observation that wild-type Co^{2+}−LuxS (but not the C84A mutant) underwent dramatic spectral changes during the catalytic cycle implies that the metal ion is directly coordinated with the substrate and

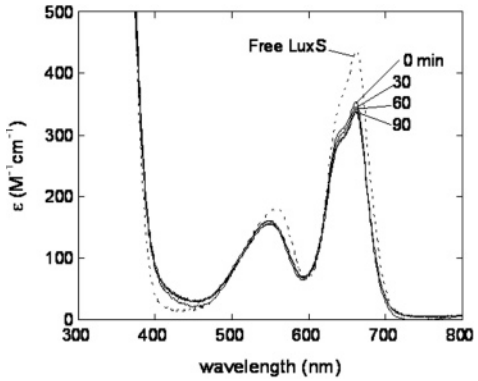

FIGURE 6: UV−vis absorption spectra of C84A Co^{2+}-BsLuxS (220 μM) in the absence and presence of 2-ketone intermediate **4** (370 μM). The LuxS and ketone **4** were rapidly mixed and the spectra were recorded at 0, 30, 60, and 90 min.

intermediates (*12*). However, the cocrystal structure of LuxS bound with SRH showed that the metal was not directly ligated to SRH (*11*). In this work, cocrystallization and absorption spectroscopy both show that a catalytic intermediate is directly coordinated with the metal center. It is reasonable to suggest that other catalytic intermediates such as the 3-ketone intermediate and the putative enediolates are also directly coordinated with the metal ion during catalysis, although further experimentation is needed to confirm this. The lack of direct binding of SRH to the metal ion can be reconciled by the hypothesis that the ribose ring form of SRH, while the dominant form under the physiological condition, is not catalytically active; rather, the open, free aldehyde form is the reactive species. The monodentate interaction between the ribulose moiety and the metal is somewhat surprising but reasonable. The enediolate formed after the abstraction of the C3 proton by Cys-84 would be expected to bind the metal ion in a bidentate fashion, as proposed for the aldose-ketose isomerases (*23*). Perhaps the LuxS active site is designed to favor the monodentate binding so that catalysis would not be trapped in the enediolate stage.

The structure and the mutagenesis studies provide additional insight into the function of active-site residues. Cys-84 has been proposed to act as the general base/acid, catalyzing the proton transfers among C1−C3 positions (*12*, *13*). The cocrystal structure of the Cys-84Ala mutant shows that the side chain of Cys-84, based on the position of Ala-84, would indeed be properly positioned for such a role. We have previously shown that mutation of Cys-84 to Ala inactivates the enzyme, whereas the C84D and C84S mutants retain residual activities (Table 2) (*13*). Thus, both structural and kinetic data are consistent with the proposed function for Cys-84. Glu-57 was proposed to catalyze the transfer of the C2 (and C3) hydroxyl proton to the C1 (and C2) oxyanion as well as serving as the general base for the final β-elimination reaction. The position of the Glu-57 side chain relative to the bound intermediate is consistent with this latter role, which is also supported by the observation that mutation of Glu-57 into Ala results in the accumulation of the 3-ketone intermediate 7 (*13*). Since its side chain carboxylate is hydrogen bonded to the C3 hydroxyl group, it can act as a general base to abstract the hydroxyl proton to form the enediolate intermediate. However, its carboxylate group is clearly too far from the C2 oxygen atom to allow a direct transfer of the proton originally derived from the C3−OH to the C2 oxyanion. Then, where does the C2 oxyanion pick up the needed proton to become a hydroxyl group? There are several other residues near the bound intermediate, Ser-6, His-11, Arg-39, and Tyr-89, all of which are highly conserved residues. Ser-6 is involved in substrate/ intermediate binding; its mutation results in moderate reduction in catalytic activity. His-11 and Arg-39 are hydrogen bonded to the C1 hydroxyl group of the 2-ketone intermediate. However, the ~1000-fold reduction in catalytic activity upon their mutation suggests that these two residues may have roles in addition to substrate/ intermediate binding. It is conceivable that His-11 acts as the general acid donating a proton to the C2 oxyanion as it departs from the metal ion. To regenerate the active enzyme, Glu-57 needs to be deprotonated, while His-11 must be protonated. We tentatively propose that Arg-39, Tyr-89, and/or several structured water molecules (Figure 3b) may serve as the proton shuttle to transfer the proton from Glu-57 to His-11.

In conclusion, the present study has provided direct evidence for the previously proposed Lewis acid function of the metal ion in LuxS-catalyzed reaction. It also provides new insights into the catalytic function of active site residues. The results should facilitate further mechanistic investigation of the enzyme and the design of selective LuxS inhibitors.

REFERENCES

1. Federle, M. J., and Bassler, B. L. (2003) Interspecies communication in bacteria, *J. Clin. Invest. 112*, 1291−1299.
2. Xavier, K. B., and Bassler, B. L. (2003) LuxS quorum sensing: more than just a numbers game, *Curr. Opin. Microbiol. 6*, 191−197.
3. Miller, C. H., and Duerre, J. A. (1968) *S*-Ribosylhomocysteine cleavage enzyme from *Escherichia coli*, *J. Biol. Chem. 243*, 92−97.
4. Surette, M. G., Miller, M. B., and Bassler, B. L. (1999) Quorum sensing in *Escherichia coli*, Salmonella *typhimurium*, and *Vibrio harveyi*: a new family of genes responsible for autoinducer production, *Proc. Natl. Acad. Sci. U.S.A. 96*, 1639−1644.
5. Schauder, S., Shokat, K., Surette, M. G., and Bassler, B. L. (2001) The LuxS family of bacterial autoinducers: biosynthesis of a novel quorum-sensing signal molecule, *Mol. Microbiol. 41*, 463−476.
6. Miller, S. T.; Xavier, K. B.; Campagna, S. R.; Taga, M. E.; Semmelhack, M. F.; Bassler, B. L.; Hughson, F. M. (2004) *Salmonella typhimurium* recognizes a chemically distinct form of the bacterial quorum-sensing signal AI-2, *Mol. Cell 15*, 677−687.
7. Chen, X., Schauder, S., Potier, N., van Dorsselaer, A., Pelczer, I., Bassler, B. L., et al. (2002) Structural identification of a bacterial quorum-sensing signal containing boron, *Nature 415*, 545−549.
8. Palmer, J, and Abeles, R. (1979) The mechanism of action of *S*-adenosylhomocysteinase, *J. Biol. Chem. 254*, 1217−1226.
9. Lewis, H. A., Furlong, E. B., Laubert, B., Eroshkina, G. A., Batiyenko, Y., Adams, J., et al. (2001) A structural genomics approach to the study of quorum sensing: crystal structures of three LuxS orthologs, *Structure 9*, 527−537.
10. Hilgers, M. T., and Ludwig, M. L. (2001) Crystal structure of the quorum-sensing protein LuxS reveals a catalytic metal site, *Proc. Natl. Acad. Sci. U.S.A. 98*, 11169−11174.
11. Ruzheinikov, S. N., Das, S. K., Sedelnikova, S. E., Hartley, A., Foster, S. J.; Horsburgh, M. J., et al. (2001) The 1.2 Å structure of a novel quorum-sensing protein, Bacillus subtilis LuxS, *J. Mol. Biol. 313*, 111−122.
12. Zhu, J., Dizin, E., Hu, X., Wavreille, A., Park, J., and Pei, D. (2003) *S*-Ribosylhomocysteinase (LuxS) is a mononuclear iron protein, *Biochemistry 42*, 4717−4726.
13. Zhu, J., Hu, X., Dizin, E., and Pei, D. (2003) Catalytic mechanism of *S*-ribosylhomocysteinase (LuxS): direct observation of ketone intermediates by ^{13}C NMR spectroscopy, *J. Am. Chem. Soc. 125*, 13379−13381.
14. Zhu, J., Patel, R., and Pei, D. (2004) Catalytic mechanism of *S*-ribosylhomocysteinase (LuxS): stereochemical course and

kinetic isotope effect of proton-transfer reactions, *Biochemistry 43*, 10166−10172.
15. Ellman, G. L. (1959) Tissue sulfhydryl groups, *Arch. Biochem. Biophys. 82*, 70−77.
16. Brünger, A. T., Adams, P. D., Clore, G. M., DeLano, W. L., Gros, P., Grosse-Kunstleve, R. W., et al. (1998) Crystallography & NMR system: A new software suite for macromolecular structure determination, *Acta Crystallogr. D54*, 905−921.
17. Jones, T. A., Zhou, J. Y., Cowan, S. W., and Kjeldgaard, M. (1991) Improved methods for building protein models in electron density maps and the location of errors in these models, *Acta Crystallogr. A47*, 110−119.
18. Schuettelkopf, A. W., and van Aalten, D. M. F. (2004) PRODRG − a tool for high-throughput crystallography of protein−ligand complexes, *Acta Crystallogr. D60*, 1355−1363.
19. Kraulis, P. (1991) MOLSCRIPT: a program to produce both detailed and schematic plots of protein structures, *J. Appl. Crystallogr. 24*, 946−950.
20. Merritt, E. A., and Bacon, D. J. (1997) Raster3D: photorealistic molecular graphics, *Methods Enzymol. 277*, 505−524.
21. Wallace, A. C., Laskowski, R. A., and Thornton, J. M. (1995) LIGPLOT: A program to generate schematic diagrams of protein−ligand interactions, *Prot. Eng. 8*, 127−134.
22. Maret, W.; Vallee, B. (1993) Cobalt as probe and label of proteins, *Methods Enzymol. 226*, 52−71.
23. Collyer, C. A.; Henrick, K.; Blow, D. M. (1990) Mechanism for aldose-ketose interconversion by d-xylose isomerase involving ring opening followed by 1,2-hydride shift, *J. Mol. Biol. 212*, 211−235.

BI0477384